

# Remapping of Digital Subtraction Angiography on a Standard Fluoroscopy System Using 2D-3D Registration

Mazen Alhrishy <sup>a</sup>, Andreas Varnavas <sup>a</sup>, Alexis Guyot <sup>a</sup>, Tom Carrell <sup>b</sup>, Andrew King <sup>a</sup>, Graeme Penney <sup>a</sup>

<sup>a</sup>Biomedical Engineering Dept., Kings College London, Kings Health Partners, London, UK.

<sup>b</sup>Vascular Surgery Dept., Guys & St Thomas NHS Foundation Trust, Kings Health Partners, London, UK.

## ABSTRACT

Fluoroscopy-guided endovascular interventions are being performed for more and more complex cases with longer screening times. However, X-ray is much better at visualizing interventional devices and dense structures compared to vasculature. To visualise vasculature, angiography screening is essential but requires the use of iodinated contrast medium (ICM) which is nephrotoxic. Acute kidney injury is the main life-threatening complication of ICM. Digital subtraction angiography (DSA) is also often a major contributor to overall patient radiation dose (81% reported). Furthermore, a DSA image is only valid for the current interventional view and not the new view once the C-arm is moved. In this paper, we propose the use of 2D-3D image registration between intraoperative images and the preoperative CT volume to facilitate DSA remapping using a standard fluoroscopy system. This allows repeated ICM-free DSA and has the potential to enable a reduction in ICM usage and radiation dose. Experiments were carried out using 9 clinical datasets. In total, 41 DSA images were remapped. For each dataset, the maximum and averaged remapping accuracy error were calculated and presented. Numerical results showed an overall averaged error of 2.50 mm, with 7 patients scoring averaged errors < 3 mm and 2 patients < 6 mm.

**Keywords:** Digital subtraction angiography (DSA), iodinated contrast media (ICM), interventional digital tomosynthesis (DTS), 2D-3D image registration, endovascular aneurysm repair (EVAR).

## 1. INTRODUCTION

Fluoroscopy-guided minimally invasive procedures such as cardiac ablation, neuroembolization, coronary artery angioplasty, and stent placement are being increasingly used in a wide range of medical specialities as they are advantageous compared to invasive surgical procedures, particularly for patients not suitable for open surgery. Advantages include substantial reduction of infection risks and a shorter recovery time because interventional fluoroscopy requires only a very small incision compared with surgical procedures.<sup>1</sup>

During fluoroscopy-guided endovascular interventions, low-dose X-ray (known as fluoroscopy screening) is used to provide guidance after inserting catheters, guide wires, or other interventional instruments into the patient's blood vessel by monitoring their movement in real-time on a set of display screens in the intervention room. However, only interventional devices and dense tissues such as bone are adequately visualized using fluoroscopy screening but not soft tissue anatomy such as the vasculature.

To enhance vasculature visualisation, iodinated contrast medium (ICM) is injected into the blood vessels, and a significantly higher X-ray dose than standard fluoroscopy screening is employed (know as angiography screening).<sup>2</sup> To visualize only the contrast flow and remove background structures, a mask image is acquired before the contrast injection and then subtracted from the subsequent angiography images resulting in a digitally subtracted angiography (DSA) image showing only the enhanced vasculature. However, a DSA image is only valid for the current interventional view, and once the C-arm is moved (translated and/or rotated), the previous DSA image does not correspond to the new interventional view. Therefore, during most procedures, DSA imaging will be repeated due to C-arm movement.

---

Email addresses: mazen.m.alhrishy@kcl.ac.uk (M.Alhrishy), andreas.varnavas@kcl.ac.uk (A.Varnavas), alexis.guyot@kcl.ac.uk (A.Guyot), tom.carrell@kcl.ac.uk (T.Carrell), andrew.king@kcl.ac.uk (A.King), graeme.penney@kcl.ac.uk (G.Penney).

ICM usage is key during interventional procedures, but nevertheless, acute kidney injury is the main life-threatening complication of ICM. ICM-induced acute kidney injury accounts for a significant number of cases of hospital-acquired renal failure,<sup>3</sup> and it was reported to be the third most common cause of hospital-acquired renal failure.<sup>4</sup> Moreover, patients with ICM-induced acute kidney injury are at high risk of in-hospital complications including a mortality rate of 20%.<sup>5</sup> This is likely to continue being the main challenge for angiography screening as chronic kidney disease and diabetes are becoming more prevalent in an ageing population.<sup>3</sup>

DSA was also found to contribute most of the patient radiation dose (81%) during endovascular interventions, even though ICM was used as sparingly as possible.<sup>2</sup> This is due to the fact that angiography screening requires a significantly higher radiation dose than standard fluoroscopy screening. With interventionists performing more and more complex procedures with longer screening times and more DSA imaging, there are growing concerns resulting from the increasing radiation exposure to both patients and the interventional team.<sup>1</sup> Radiation exposure may well be set to rise dramatically in the coming years.<sup>6</sup>

New imaging techniques to minimize the need for repeated DSA and subsequently reducing the volume of nephrotoxic ICM and radiation exposure -while maintaining the necessary image quality to perform complex procedures- are required.<sup>2, 6</sup> This is particularly significant for patients with renal insufficiency where ICM increases mortality rates and adverse events, and for patients at high risk of radiation adverse response such as patients with a previous high-dose from an earlier treatment. Techniques to minimize repeated DSA mainly include using 2D-3D registration algorithms to provide a 3D preoperative overlay into the 2D intraoperative fluoroscopy images during fluoroscopy-guided interventions.<sup>7</sup> However, there are issues with intraoperative deformation.<sup>8</sup>

The clinical need to minimize repeated DSA imaging has motivated this submission to investigate minimally-nephrotoxic imaging methods during interventional fluoroscopy. In this submission, we propose the use of 2D-3D image registration to facilitate DSA remapping using a standard fluoroscopy system. This allows repeated ICM-free DSA and results in minimal ICM usage and reduced radiation dose.

In the following we firstly provide a brief overview of standard digital subtraction angiography. We then explain how our novel methods work by using a preoperative CT volume and 2D-3D registration. Experiments are then described, and results presented using data from 9 patient datasets.

## 2. OVERVIEW OF DIGITAL SUBTRACTION ANGIOGRAPHY

As previously mentioned, blood vessels are not well visualized using standard fluoroscopy screening. This is because the difference in attenuation coefficients between blood and surrounding soft tissues is very small. To render the vessel's lumen opaque, it is necessary to use a contrast medium with a high attenuation coefficient, such as ICM, which relies on iodine for its radio-opacity. High-contrast background objects are then subtracted from the image as they will obscure the lower-contrast blood vessels containing dilute iodine. Once the high-contrast structures have been removed, the subtracted image (i.e. DSA image) can be enhanced using display windowing techniques. Figure 1 illustrates the basic digital subtraction angiography principle which can be divided into these steps:

1. A mask image is acquired before administration of ICM (Fig. 1.a).
2. ICM is injected intra-arterially and an angiography screening showing the contrast flow over time is obtained.
3. All individual frames in the angiography screening are subtracted, pixel by pixel, from the mask image to remove background high-contrast structures (Fig. 1.b<sub>1</sub> ~ b<sub>n</sub>).
4. The subtracted frames are then used to generate a DSA image (Fig. 1.c), using the maximum intensity projection (MIP) method. In MIP, only pixels with the highest intensity values throughout the subtracted frames are projected into a single image.

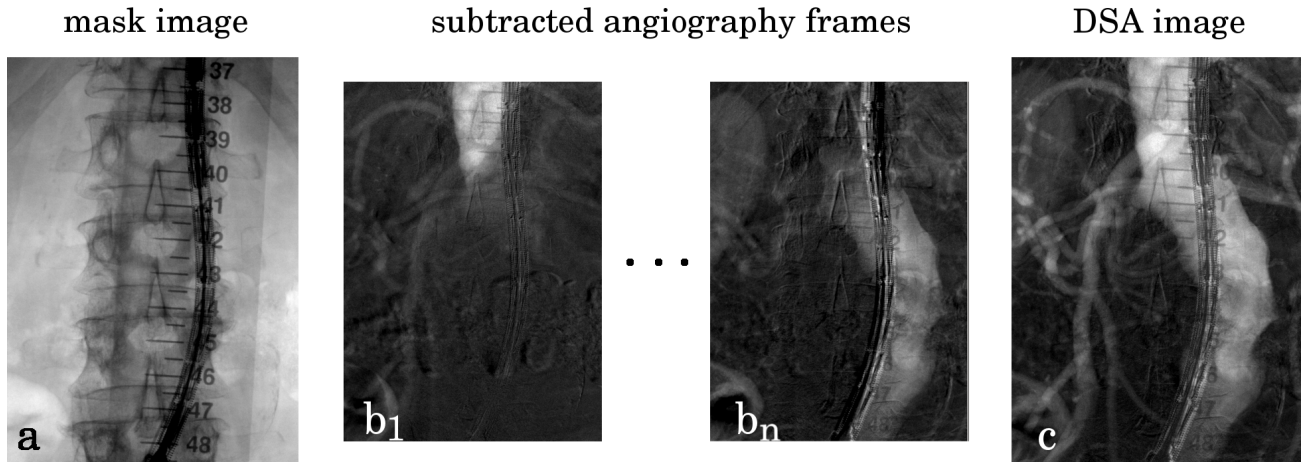


Figure 1. Basic digital subtraction angiography. The mask image (a) is subtracted -pixel by pixel- from all individual frames in the angiography screening ( $b_1 \sim b_n$ ). A DSA image (c) is then generated from the subtracted frames using the maximum intensity projection method.

If no ICM was injected, and if no soft tissues motion existed between the mask and the subsequent angiography images, the DSA image will be blank. However, in the presence of ICM, the DSA image will show the iodinated vascular structures. The main limitation of this technique is movement artefact which appears if motion occurs between pre- and post- ICM injection images. If such motion exists, the mask subtraction will not totally cancel out all background structures, and movement artefacts appear in the DSA image.

### 3. THE PROBLEM OF REMAPPING PROJECTION DATA

Figure 2 illustrates the 2D geometry of perspective projection used in fluoroscopy imaging. In ‘a’ and ‘b’ the X-ray source and detector are moved around the patient from view 1 to view 2 to acquire a new 2D projection image.

As shown in ‘a’, remapping the first image into the second view direction cannot be accurately achieved using only knowledge of the relative view directions 1 and 2. Additional knowledge is required: information on the depth position (distance along ray path) of the anatomical features depicted inside the patient. In Fig. 2.a, the gray circle inside the patient is projected into the detector along the blue line using the first view direction. However, when the source is moved to the second view direction, the blue circle cannot be remapped to view 2 without extra information on the gray circle’s position inside the patient. This is because the blue circle might be projected from any point along the blue line intersecting the patient, such as the points marked with +, which if used for remapping along the red lines will result in multiple possible locations of the red circle on view 2.

If all the 2D image information can be projected back to a single accurately known 2D surface, such as the one depicted in Fig. 2.b, then the image can be remapped accurately into the second view. In Fig. 2.b, the projected blue square, triangle, and circle using view 1 can be correctly remapped to view 2 using the position information provided by the remapping surface intersecting these features inside the patient. However, as the depth information becomes more three-dimensional (i.e. does not just originate from a single 2D remapping surface), and as errors arise in positioning the 2D surface, then errors will occur in the remapping process.

The ability to define such a surface accurately is essential for a correct perspective projection remapping. We propose defining a remapping surface inside the preoperative CT volume and then matching this surface to the patient using 2D-3D registration during intervention. This surface is then used to remap a DSA image to a new view direction as described in the next section.

### 4. MATERIALS AND METHODS

This section begins by defining the three coordinate systems used. Then, it gives an overview of the employed 2D-3D registration algorithm, and finally explains how this algorithm enables DSA Remapping on a standard fluoroscopy system.

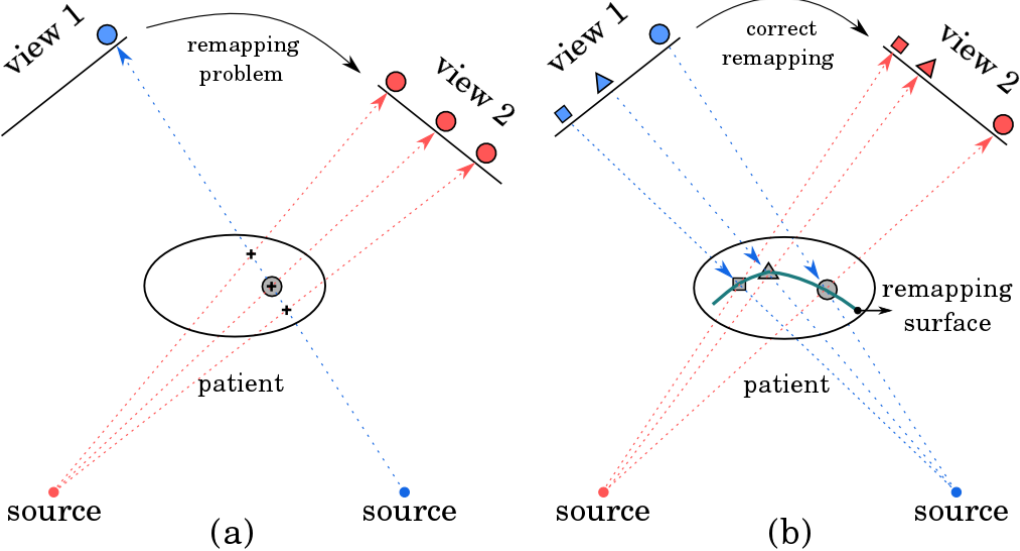


Figure 2. The problem of remapping projection data. a) the 2D blue circle cannot be remapped from view 1 to view 2 without knowing it's 3D position (i.e. gray circle) along the blue ray path. b) If a remapping surface is known, the blue square, triangle, and circle can be correctly remapped from view 1 to view 2.

#### 4.1 Coordinate Systems Definition

The following coordinate systems are used in this submission:

- $\mathbf{X}_{3D}$ : this defines 3D positions with respect to the X-ray fluoroscopy set (i.e. X-ray source and detector). Coordinates in  $\mathbf{X}_{3D}$  are denoted with the capital letters ( $X, Y, Z$ ).
- $\mathbf{CT}_{3D}$ : this defines 3D positions in the preoperative CT volume. Coordinates in  $\mathbf{CT}_{3D}$  are denoted with the small letters ( $x, y, z$ ).
- $\mathbf{I}_{2D}$ : this defines 2D positions in the X-ray projection image. Coordinates in  $\mathbf{I}_{2D}$  are denoted with the small letters ( $u, v$ ).

#### 4.2 Overview of the 2D-3D Registration Algorithm

Our DSA remapping method uses a well established intensity-based 2D-3D registration algorithm.<sup>9,10</sup> The algorithm aligns a preoperative CT volume coordinate system ( $\mathbf{CT}_{3D}$ ) with the fluoroscopy set coordinate system ( $\mathbf{X}_{3D}$ ) to enhance guidance during interventions as seen in Fig. 3. This system has been regularly used for elective endovascular aortic repair (EVAR) at St Thomas' hospital (London, UK) as part of a clinical trial (National Research Ethics Service approval 09/H0707/64).

The algorithm generates digitally reconstructed radiographs (DRRs) by casting rays through an automatically segmented vertebra from the preoperative CT, and integrating voxel values above a threshold (200 HU) along each ray. DRRs are then compared with the intraoperative fluoroscopy images using a gradient difference similarity measure.<sup>9</sup>

Figure 3 illustrates the 10 degrees of freedom involved in perspective projection transformation. These can be split up into 3 matrices:

- A  $3 \times 4$  perspective matrix  $P(c_s, l_s, k_1, k_2)$ , where  $c_s$  and  $l_s$  mark the 2D positions on the imaging plane where the normal to that plane goes through the X-ray source.  $k_1$  and  $k_2$  are the source to detector distance divided by the 2D image pixel sizes.
- A  $4 \times 4$  rotational matrix  $R(\theta_X, \theta_Y, \theta_Z)$ , where  $\theta_X$ ,  $\theta_Y$ , and  $\theta_Z$  represent the orientation of  $\mathbf{CT}_{3D}$  with respect to  $\mathbf{X}_{3D}$ .

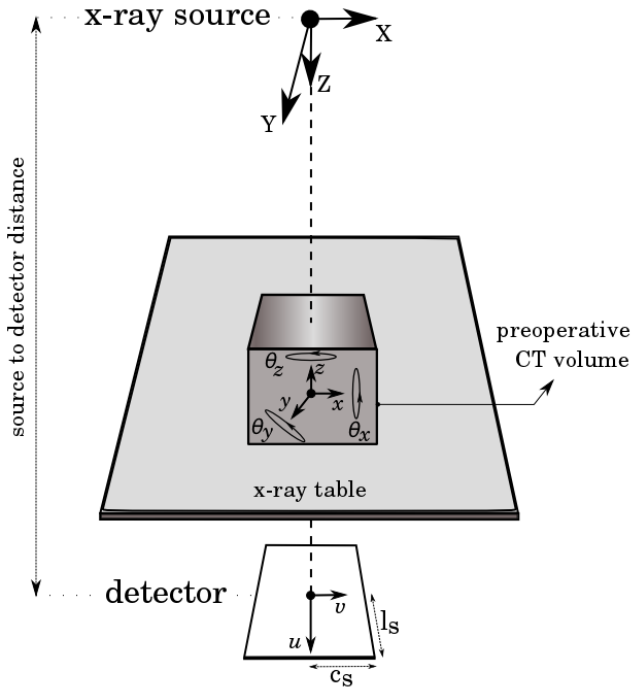


Figure 3. A preoperative CT volume is registered with the intraoperative image using a 2D-3D registration algorithm.  $c_s$  and  $l_s$  mark the positions of the interception between the ray projected from the X-ray source into the imaging plane.  $\theta_X$ ,  $\theta_Y$ , and  $\theta_Z$  represent the imaged object orientation, while  $X$ ,  $Y$ , and  $Z$  represent its position with respect to the fluoroscopy set coordinate system ( $\mathbf{X}_{3D}$ ).

- A  $4 \times 4$  translation matrix  $T(X, Y, Z)$ , where  $X$ ,  $Y$ , and  $Z$  represent the position of  $\mathbf{CT}_{3D}$  with respect to  $\mathbf{X}_{3D}$ .

These 3 matrices can be combined to produce a projection transformation matrix  $M(W)$  as shown in the following equation (Eqn. 1):

$$M(W) = P(c_s, l_s, k_1, k_2)R(\theta_X, \theta_Y, \theta_Z)T(X, Y, Z) \quad (1)$$

Matrix  $M(W)$  relates positions (represented as homogeneous coordinates) between  $\mathbf{CT}_{3D}$  and  $\mathbf{I}_{2D}$ , as shown in Eqn. (2), where  $\lambda$  is a scaling factor:

$$M(W)(x, y, z, 1)^T = \lambda(u, v, 1)^T \quad (2)$$

Therefore,  $M(W)$  can be used to project a 3D point in  $\mathbf{CT}_{3D}$  to a 2D point in  $\mathbf{I}_{2D}$ , or to transform a 2D point in  $\mathbf{I}_{2D}$  to a 3D line in  $\mathbf{CT}_{3D}$ .

#### 4.3 Using the 2D-3D Registration Algorithm to Facilitate DSA Remapping

This paper's novelty lies in the use of the previously highlighted 2D-3D registration to facilitate DSA remapping. Figure 4 demonstrates how the 2D-3D registration algorithm enables DSA remapping. This begins at the top with the input images: a) a DSA mask and b) a DSA image ( $I_{DSA}$ ) produced from a posterior-anterior view, c) a new fluoroscopy image ( $I_{FL}$ ) acquired after the C-arm was moved, and d) the preoperative CT scan with the remapping surface defined inside. Images 'a', 'c', and 'd' are input into the 2D-3D registration algorithm which calculates the 2D-3D transformations between the CT scan  $(x, y, z, 1)^T$  and both the DSA image  $(u, v, 1)^T_{DSA}$  and the new fluoroscopy image  $(u, v, 1)^T_{FL}$  i.e.:

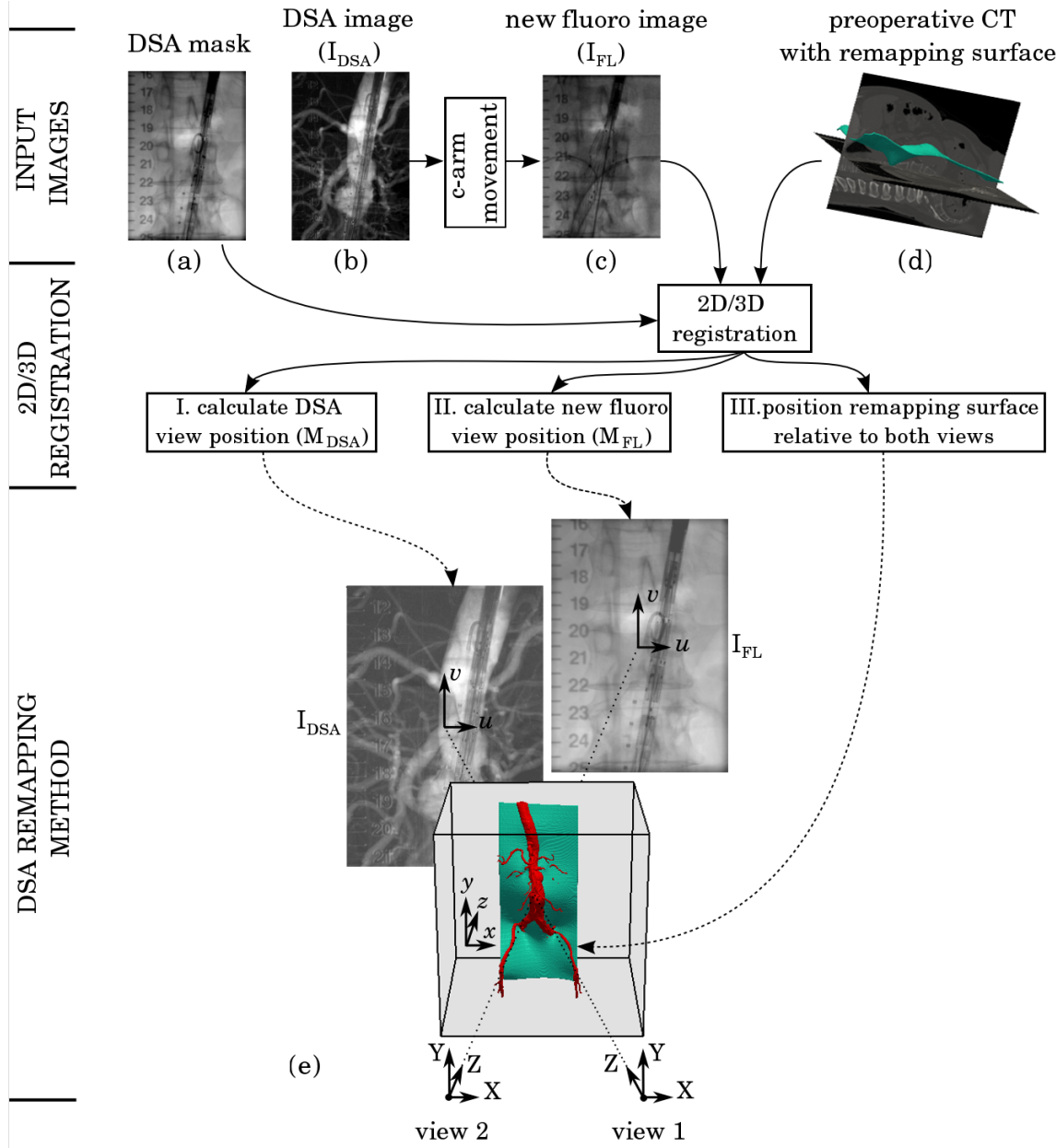


Figure 4. Flow diagram showing how the 2D-3D registration algorithm enables DSA remapping. Top shows input images: a) DSA mask, b) DSA image, c) new fluoroscopy image acquired after the C-arm was moved to a new view, and d) a preoperative CT with the remapping surface. Middle and bottom shows the 2D-3D registration which enables calculation of view directions and positioning of patient-vasculature-specific remapping surface (d).

$$M_{DSA}(x, y, z, 1)^T = \lambda(u, v, 1)^T_{DSA} \quad (3)$$

$$M_{FL}(x, y, z, 1)^T = \lambda(u, v, 1)^T_{FL}$$

The three boxes in Fig. 4 show the subsequent stages to the 2D-3D registration which provide the necessary information to carry out DSA remapping. The Roman numerals labelling each box correspond to the following processes:

- I. Calculate DSA view position: the transformation  $M_{DSA}$  to position  $I_{DSA}$  in relation with  $\mathbf{CT}_{3D}$  is determined using the DSA mask. Both the DSA mask and DSA image have the same transformation as they are acquired in a single angiography screening from the same view direction.
- II. Calculate new fluoroscopy view position: the transformation  $M_{FL}$  to position  $I_{FL}$  in relation with  $\mathbf{CT}_{3D}$  is determined.
- III. The transformations  $M_{DSA}$  and  $M_{FL}$  can position the preoperatively defined remapping surface inside the CT volume with respect to both  $I_{DSA}$  and  $I_{FL}$ , enabling remapping to occur on a patient-vasculature-specific surface.

#### 4.4 DSA Remapping Process

In Sec. 4.3 we listed the information provided by the 2D-3D registration to enable DSA remapping. In this section, we describe how this information enables DSA remapping. This is detailed in the below steps (I, II, III, IV, V) illustrated in Fig. 5, where the Roman numerals in the figure correspond to the following steps:

- I. Segmenting a remapping surface from the preoperative CT volume. The surface should contain the blood vessels of clinical interest to be remapped.
- II. Registering the CT volume with both images,  $I_{DSA}$  and  $I_{FL}$ , using the 2D-3D registration algorithm as described in Sec. 4.3. The registration allows spatial positioning of  $I_{DSA}$  and  $I_{FL}$  in relation to the segmented CT remapping surface as was described in Sec. 4.3.I & II.
- III. Back projecting rays from each of the DSA image pixels (i.e.  $I_{DSA}(u, v)$ ) using  $M_{DSA}$ , and calculating the 3D positions in  $\mathbf{CT}_{3D}$  where the rays intercept the remapping surface (i.e.  $CT(x, y, z)_{int}$ ).
- IV. Projecting rays from the 3D interception positions  $CT(x, y, z)_{int}$  to  $I_{FL}$  to acquire the 2D interception position in  $\mathbf{I}_{2D}$  (i.e.  $I_{FL}(u, v)$ ). This is done using the transformation  $M_{FL}$ .
- V. Finally, the intensity at each DSA image pixel  $I_{DSA}(u, v)$  is remapped onto the 2D interception position  $I_{FL}(u, v)$  corresponding to the same pixel. This automatically produces a remapped DSA image corresponding to the current fluoroscopy view.

#### 4.5 DSA Remapping Errors

As discussed in Sec. 3, remapping a projection image into a new view requires knowledge on the depth position of the anatomical features. Our method provides such knowledge by defining a remapping surface inside the CT volume to intersect features of interest. The method assumes features to lie on a single 2D surface, and that the surface can be positioned correctly. However, when these assumptions are violated three types of errors arise:

- I. We define type 1 error ( $E_1$ ) to occur as a result of the thickness of the feature being remapped (i.e. feature's size along the  $z$  direction in  $\mathbf{CT}_{3D}$ ).  $E_1$  is a function of the feature's thickness and changes in the ray paths ( $\Delta rayPath$ ) along that feature when the C-arm is moved to a new view direction, such as:

$$E_1 = f(\text{thickness}, \Delta rayPath) \begin{cases} E_1 = 0, & \text{if features lie completely on the remapping surface.} \\ E_1 > 0, & \text{otherwise.} \end{cases} \quad (4)$$

When the entire feature lies on the remapping surface, then, the ray paths along that feature are similar from any view direction and  $E_1 = 0$ . However, when the feature's thickness increases, the changes in the ray paths increase when the C-arm is moved, and thus,  $E_1$  increases as seen in Fig. 6. In 'a' and 'b', two images of an aneurysmal aorta are acquired from two different view directions. In both cases, the projected ray to view 2 (red arrow) does not intersect the same part of the aorta as the projected ray from view 1 (blue arrow). This causes type 1 error in the features' position between the remapped image from view

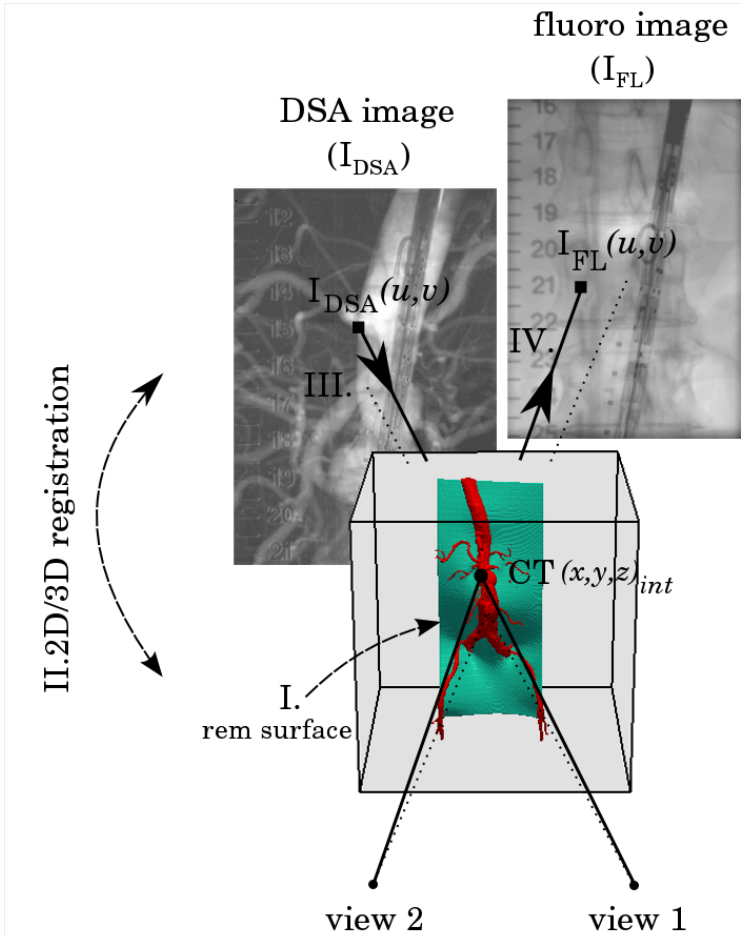


Figure 5. DSA remapping process shown in detail for one pixel in the DSA image:  $I_{DSA}(u, v)$ . A ray is back projected from  $I_{DSA}(u, v)$  into the remapping surface using  $M_{DSA}$ . The 3D interception position  $CT(x, y, z)_{int}$  is then projected into the fluoroscopy image using the transformation  $M_{FL}$  to acquire the 2D interception position in the fluoroscopy image  $I_{FL}(u, v)$ . Finally, the intensity at  $I_{DSA}(u, v)$  is remapped onto  $I_{FL}(u, v)$ .

1 and the new image from view 2 when overlaid. In addition, in ‘b’, the red arrow intersection with the aorta (red solid line) is further away from the blue arrow intersection (blue solid line) when compared to ‘a’, this is because the feature’s thickness in ‘b’ is much larger than in ‘b’.

II. We define type 2 error ( $E_2$ ) to be due to errors in positioning the remapping surface.  $E_2$  is a function of the 2D-3D registration error ( $E_{reg}$ ),<sup>9</sup> and the intraoperative deformation ( $D_{ef}$ ),<sup>8</sup> such as:

$$E_2 = f(E_{reg}, D_{ef}) \begin{cases} E_2 = 0, & \text{if } E_{reg} = 0 \text{ and } D_{ef} = 0. \\ E_2 > 0, & \text{otherwise.} \end{cases} \quad (5)$$

$E_{reg}$  results from misaligning  $\mathbf{CT}_{3D}$  with  $\mathbf{X}_{3D}$  as mentioned in Sec. 4.2 (i.e. errors in  $R(\theta_X, \theta_Y, \theta_Z)$  and  $T(X, Y, Z)$ ). The translation error along the Z axis (see Fig. 3) is the largest error observed when compared to the other translations and rotations errors ( $\sim 5$  mm Vs.  $\sim 0.5$  mm respectively<sup>9</sup>). Therefore, errors in positioning the remapping surface along the Z axis may occur as shown in Fig. 7.a. In ‘a’, where no deformation occurs ( $D_{ef} = 0$ ), the blue arrow intersects the CT volume at the wrong depth position because of the Z translation error causing  $E_2$  error.

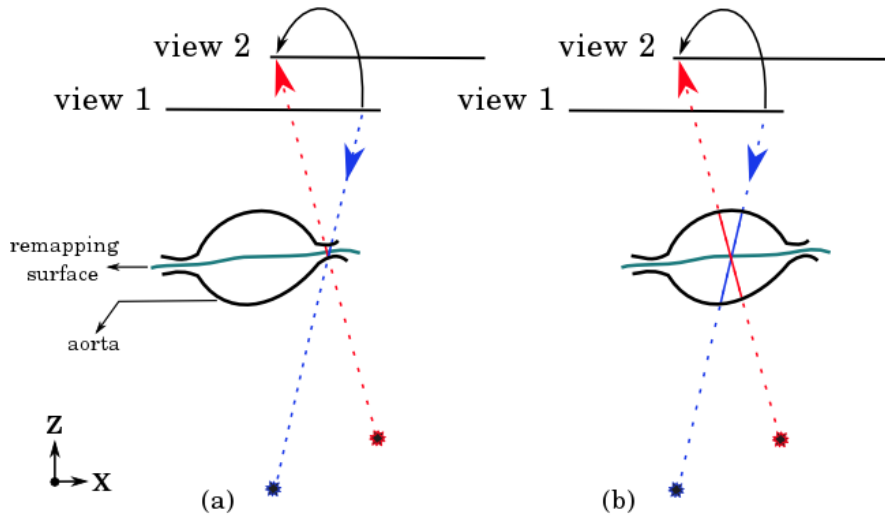


Figure 6. Type 1 error ( $E_1$ ) as a function of the feature's thickness and changes in ray paths. Both 'a' & 'b' show images of the aorta acquired from two different views with the red arrow intersecting a different part of the aorta (solid red) than the blue arrow (solid blue), causing type 1 error. In 'b', however, the solid red line is further away from the solid blue line when compared to 'a'.

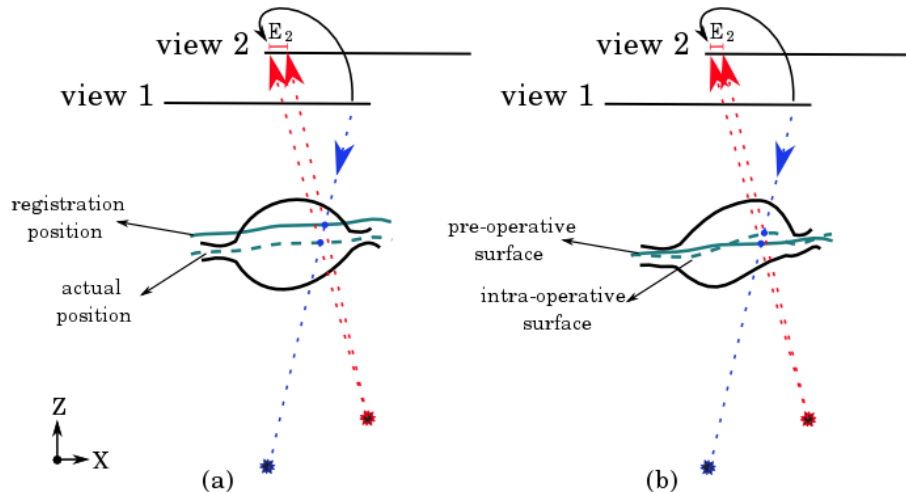


Figure 7. Type 2 error ( $E_2$ ) relation with a) the 2D-3D registration errors ( $E_{reg}$ ), and b) the intraoperative deformation ( $D_{ef}$ ). In both cases two images of the aorta are acquired from different views. The blue arrow intersects the CT volume at the wrong depth position causing  $E_2 > 0$  in both 'a' & 'b'.

$D_{ef}$  is a common issue in all methods that employ preoperative anatomy for overlay.  $D_{ef}$  might occur because of the movement of the stiff wires and delivery systems inside the aorta during intervention ( $< 10$  mm<sup>8</sup>). This might cause errors in the position of the remapping surface as illustrated in Fig. 7.b. In 'b', where no registration error occurs ( $E_{reg} = 0$ ), the blue arrow intersects the CT volume at the wrong depth position because of the intraoperative deformation of the remapping surface causing  $E_2$  error.

- III. We define type 3 error ( $E_3$ ) to be due to non-rigid movement of features of interest (relative to the vertebrae on which registration is based) between the time the DSA image ( $I_{DSA}$ ) was acquired and the time the new fluoroscopy image ( $I_{FL}$ ) was acquired.  $E_3$  is a function of the different stages during an intervention which exhibit different amounts of intraoperative deformation depending on the type of the interventional devices present.

$E_3$  is a minimum when  $I_{DSA}$  and  $I_{FL}$  are acquired during the same stage of the intervention as the amount of deformation should be similar for both images. However, if  $I_{DSA}$  and  $I_{FL}$  are acquired during different stages, then  $E_3$  increases as the two images experience different amounts of deformation. In addition, the delivery device with the undeployed stent-grafts is the main cause of deformation, therefore, if  $I_{DSA}$  is acquired when the delivery device is present and  $I_{FL}$  when it was not,  $E_3$  is a maximum.

## 5. DATA AND EXPERIMENTS

Experiments were carried out using data from 9 patients who underwent elective EVAR in St Thomas' hospital (London, UK). Data was processed offline, i.e. not during procedure and was approved by the National Research Ethics Service with informed patient consent.

Each dataset had a preoperative diagnostic CT scan, acquired on a variety of machines depending on the referring hospital, with voxel sizes ranging from  $0.683 \times 0.683 \times 0.7 \text{ mm}^3$  to  $1 \times 1 \times 1 \text{ mm}^3$ . Each dataset also had a number of intraoperative images (fluoroscopy screening, angiography screening, and DSAs) acquired on a Siemens FP20 system with a low frame rate ranging from 2 fps to 7 fps.

### 5.1 Experiment

For each patient, the aorta was segmented from the preoperative CT volume using a semi-automatic method in ITK-SNAP.<sup>11</sup> The remapping surface was then defined by picking points along the midline of the aorta, iliac and renal arteries and then producing a surface using thin-plate-spline interpolation.<sup>12</sup> An example of such a remapping surface can be seen in Fig. 8 from different views: a) anterior-posterior, b) lateral, and c) posterior-anterior. This surface was chosen to remap blood vessels of interest, i.e. the aorta, and renal and iliac arteries.

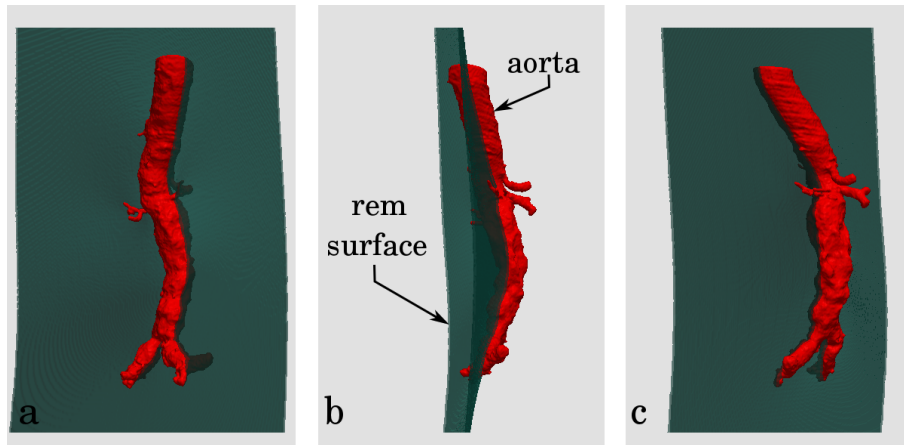


Figure 8. Illustration of a surface used for DSA remapping from different anatomical views: a) anterior-posterior, b) lateral, and c) posterior-anterior. The surface is defined along the aorta using thin-plate-spline interpolation.

For each dataset, a DSA image produced from an anterior-posterior view at an early stage of the intervention was chosen to be remapped. These DSA images show the delivery devices with the undeployed stent-grafts as well as vasculature. DSA remapping, as described in Sec. 4.4, was then carried out to remap the chosen DSA image to a number of fluoroscopy images acquired at different stages of the intervention after C-arm movement (but approximately from anterior-posterior views).

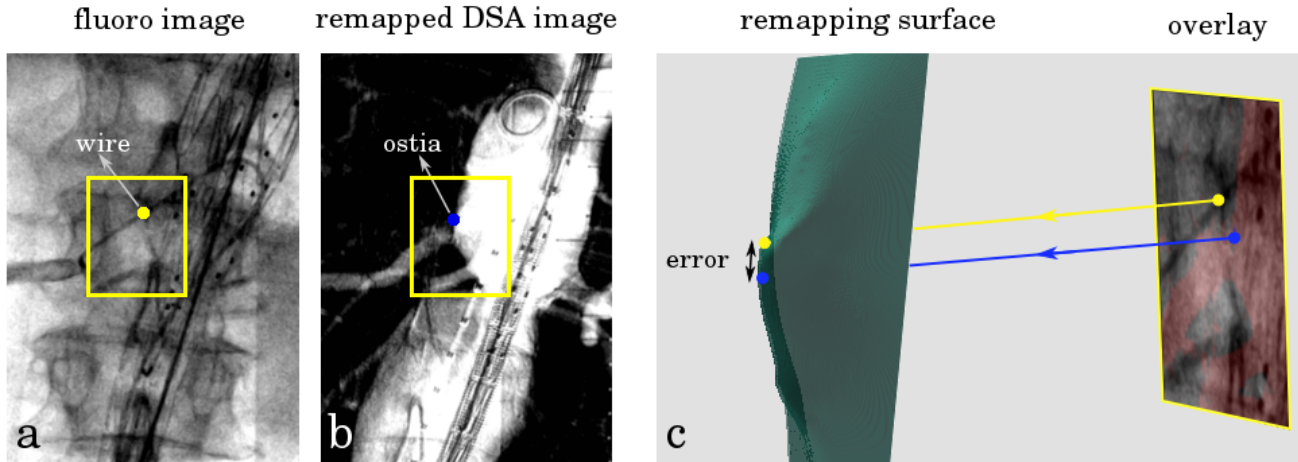


Figure 9. Illustration of the used validation method. a) the fluoroscopy image with a yellow dot marking the guide-wire. b) the remapped DSA image with a blue dot marking the renal ostium. c) rays are back projected from the centres of the blue and yellow dots in the overlay image into the remapping surface using the transformation  $M_{FL}$ , and the error is calculated in mm in  $\text{CT}_{3D}$ .

## 5.2 Validation Experiments

Validation images were chosen for each dataset which clearly showed the position of the renal arteries, either by the position of a guide-wire or a stent-graft, or by the use of ICM. Overlay accuracy was then calculated at a clinically relevant position: the renal ostium in both the fluoroscopy image ( $I_{FL}$ ) and the remapped DSA image ( $I_{DSA(rem)}$ ), as shown in Fig. 9.

In Fig. 9, where a guide-wire is used, an error value of zero was recorded if the wire in  $I_{FL}$  (yellow dot in 'a') went through the  $I_{DSA(rem)}$  renal ostium (blue dot in 'b'). Otherwise, the error value was calculated as described in Fig. 9.c. In 'c', rays are back projected from the overlay image into the remapping surface using the transformation  $M_{FL}$ . The distance (i.e. error) between the two points of interception with the surface is then calculated in mm in  $\text{CT}_{3D}$  using the formula  $\sqrt{(x_1 - x_2)^2 + (y_1 - y_2)^2 + (z_1 - z_2)^2}$ . This method allows the error to be calculated in real anatomical distance (i.e. mm) not a projected error (i.e. pixels).

In the case where a stent-graft or an ICM was used, the middle-points of the renal ostia were located in both  $I_{FL}$  and  $I_{DSA(rem)}$ , and the same method of back projection was used to calculate the error in mm. For each dataset and in all cases (i.e. wire/stent/ICM), locations of the renal ostia were located visually by 2 observers independently. Two sets of errors were then calculated and averaged for each dataset.

## 6. RESULTS

Figure 10 shows results from patients 2,4, and 8 respectively: a) the DSA image ( $I_{DSA}$ ), b) the fluoroscopy image ( $I_{FL}$ ), c) the remapped DSA image ( $I_{DSA(rem)}$ ), and d)  $I_{DSA(rem)}$  overlaid onto  $I_{FL}$  in red, with the renal ostia marked with blue dots in  $I_{DSA(rem)}$  and yellow dots in  $I_{FL}$ . Presented patients were chosen to have remapping errors which covered the full range of observed average errors: 0.82 mm, 2.92 mm, and 5.52 mm, respectively.

For each patient, the remapping accuracies, as described in sec. 5.2, were calculated for all images and averaged. Table 1 lists the number of DSA remappings for each patient, and the maximum and averaged remapping errors. The overall number of remappings performed and averaged error are also presented in bold text. Numerical results showed an overall error average of 2.50 mm over 41 remapped images, with 1 case scoring zero error and 6 other cases scoring averaged errors  $< 3$  mm. For 2 patients, larger averaged errors ( $> 4$  mm) were observed. In 5 patients, large maximum errors ( $> 4$  mm) were observed with patient 8 scored the highest maximum (11.57 mm) and averaged (5.52 mm) errors.

The 2D-3D registration was performed on a computer with two NVidia GTX 690 graphic cards with each card containing two GPUs. A single 2D-3D registration was completed in 1.25 sec, and the remapping software took around 1 sec. Thus, the entire remapping process time was around 3.5 sec for each fluoroscopy image.

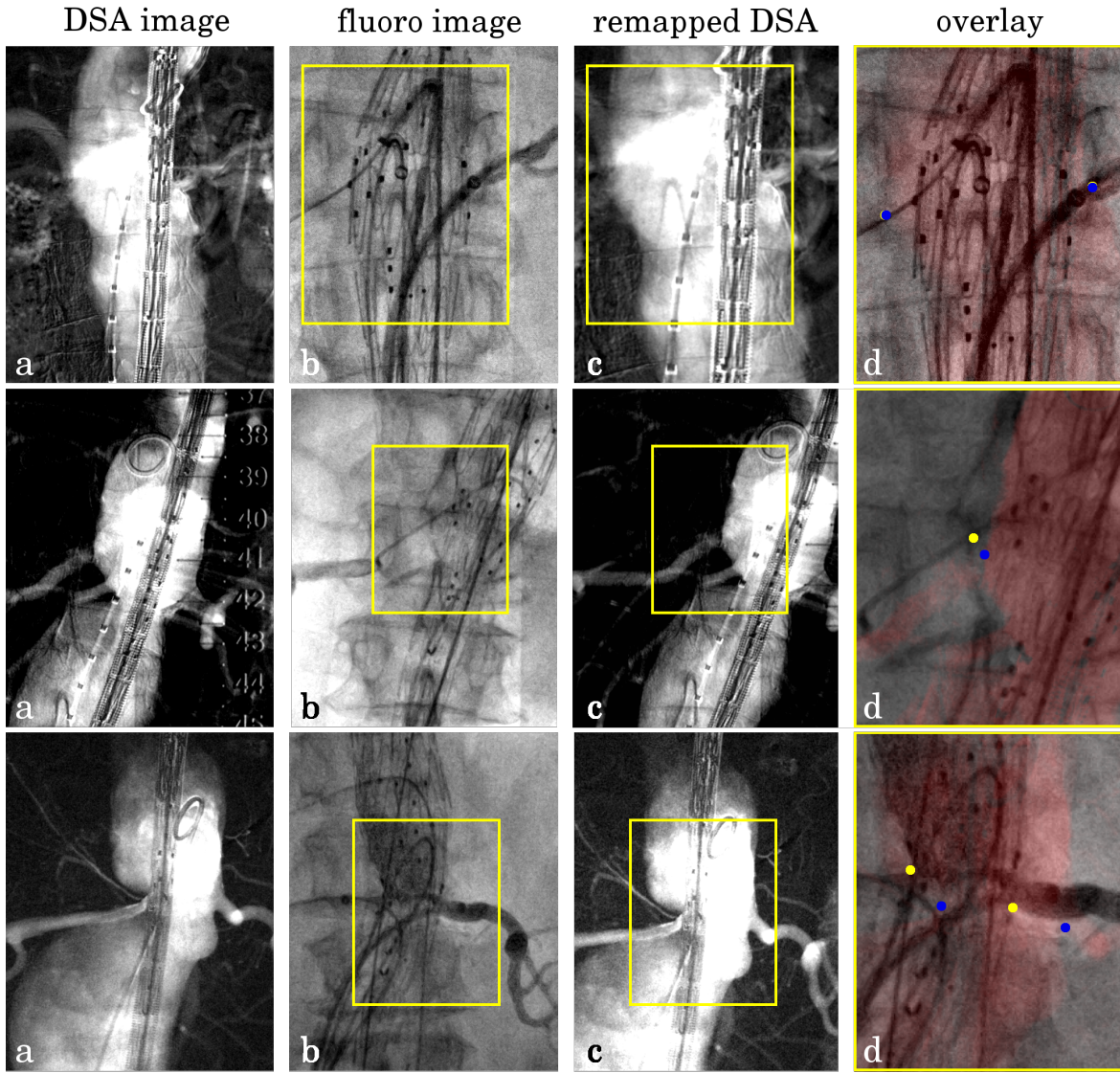


Figure 10. Representative results from patients 2, 4, and 8 respectively. a)  $I_{DSA}$ , b)  $I_{FL}$ , c)  $I_{DSA(rem)}$ , and d)  $I_{DSA(rem)}$  overlaid onto  $I_{FL}$  in red, with the renal ostia marked with blue dots in  $I_{DSA(rem)}$  and yellow dots in  $I_{FL}$ .

## 7. DISCUSSION AND CONCLUSIONS

We have developed a novel imaging technique to minimize repeated DSA imaging during interventional fluoroscopy. Consequently, the volume of nephrotoxic ICM and radiation exposure would be reduced, allowing interventionist to perform more complex procedures with longer screening times. The technique is particularly beneficial for patients with renal insufficiency and/or patients at high risk of radiation adverse response. We propose that DSA remapping could find a role alongside DSA imaging, replacing DSA imaging where appropriate, while using DSA for critical points in the procedure.

Our proposed method calculates the relative view positions between the DSA image and the new fluoroscopy image acquired after a C-arm movement using 2D-3D registration. Therefore, the method is able to work with any existing fluoroscopy system without any hardware alterations, and does not require mechanical tracking of the C-arm nor calibration. The method only requires the use of a preoperative CT scan, which is already available as a part of the routine planning for EVAR procedures. Moreover, the remapping surface can be defined preoperatively inside the CT volume to intersect features of interest. This then enables DSA remapping to automatically enhance vasculature without the need for any input from the interventional team during intervention which could interrupt the clinical work-flow.

Table 1. The number of DSA remappings performed, the maximum error and the averaged remapping error in mm for each patient.

	number of remappings	maximum error (mm)	averaged error (mm)
Patient 1	5	3.39	1.79
Patient 2	7	1.34	0.82
Patient 3	5	4.41	2.46
Patient 4	4	4.55	2.92
Patient 5	3	0	0
Patient 6	2	3.1	1.77
Patient 7	6	4.64	2.61
Patient 8	6	11.57	5.52
Patient 9	3	6.19	4.58
<b>Overall</b>	<b>41</b>	<b>11.57</b>	<b>2.50</b>

As described in Sec 4.5, the proposed method can only employ an accurately positioned single 2D surface for remapping. The aorta does not just originate from a single 2D remapping surface. However, for small structures of the aorta such as the renal ostia, this is not expected to have a large effect on type 1 error (Sec. 4.5.I). The robustness of the registration algorithm to accurately position the CT volume has been tested and reported.<sup>9,10</sup> The Z translation error ( $\sim 5$  mm<sup>9</sup>) would have a smaller effect on type 2 error (Sec. 4.5.I) compared to the intraoperative deformation ( $< 10$  mm<sup>8</sup>). This is because the deformation could result in use of a remapping surface at a further distance from the intraoperative position of the clinical features.

Nevertheless, during fluoroscopy interventions, surgeons are mostly interested in using overlays after the delivery system was inserted, which is known to cause the largest amount of deformation.<sup>8</sup> Unlike 2D-3D registration methods which use preoperative overlays acquired before the deformation has occurred, our method uses an intraoperative overlay (i.e. a DSA image) acquired after the delivery system was inserted and caused deformation. Therefore, when the new fluoroscopy images are acquired with the delivery system still present, the remapped DSA image should have a similar amount of deformation resulting in a better overlay accuracy than that in 2D-3D registration overlays. Future work is to investigate this overlay accuracy improvement.

Results presented in Tab. 1 showed an averaged remapping error of 2.50 mm over 41 remappings performed. Error variations across different remappings for the same patient were observed. This can be explained by the fact that remappings were performed at different stages of the procedure for each patient (see Sec. 5.1). Thus, the aorta experienced different amounts of intraoperative deformation depending on the type of interventional devices present. When overlaying the segmented aorta into the remapped DSA image with the highest overlay error (i.e. 11.57 mm for patient 8), this case was found to have the biggest intraoperative deformation compared to the other DSA remappings for the same patient, which explains the big maximum error reported for patient 8.

Future work is to study the effect of the different error types on the overlay accuracy. Warping the preoperative aorta to match the intraoperative scene before segmenting the remapping surface can also be investigated by employing a non-rigid 2D-3D image registration algorithm (e.g.<sup>13</sup>) to account for the intraoperative deformation. The potential use of DSA remapping during a series of procedures will also be investigated. Interventionist will be able to view the remapped DSA images during the procedure, and they will examine the remapped DSA image quality of desired clinical features and its potential to aid guidance. Moreover, the reduction in ICM usage and radiation dose will be estimated.

In summary, a novel method to minimize repeated DSA has been presented. The method employs a 2D-3D registration algorithm to enable DSA remapping into a new fluoroscopy image using standard interventional equipment. This allows repeated ICM-free DSA and reduced radiation dose. 41 DSA images were remapped. Numerical results showed an overall remapping accuracy error of 2.50 mm with one case scoring zero error and 6 other cases scoring averaged errors  $< 3$  mm. For 2 patients, larger averaged errors ( $> 4$  mm) were observed.

## 8. ACKNOWLEDGMENTS

The authors acknowledge financial support from King's Overseas Research Studentship (KORS), The Cardiovascular Healthcare Technology Co-operative (HTC) Innovation, Guy's and St Thomas' Charity, and the department of health via the National Institute for Health Research (NIHR) comprehensive Biomedical Research Centre award to Guy's & St Thomas' NHS Foundation Trust in partnership with King's College London and Kings College Hospital NHS Foundation Trust. Thanks also go to all clinical staff at St. Thomas' Hospital who aided this research.

## REFERENCES

- [1] Miller, D., "Interventional fluoroscopy: reducing radiation risks for patients and staff," *J. Vasc. Interv. Radiol.* **20**(7), 274–274 (2009).
- [2] Patel, A., Gallacher, D., Dourado, R., Lyons, O., Smith, A., Zayed, H., Waltham, M., Sabharwal, T., Bell, R., Carrell, T., et al., "Occupational radiation exposure during endovascular aortic procedures," *Eur. J. Vasc. Endovasc.* **46**(4), 424–430 (2013).
- [3] McCullough, P. A., "Contrast-induced acute kidney injury," *J. Am. Coll. Cardiol.* **51**(15), 1419–1428 (2008).
- [4] Nash, K., Hafeez, A., and Hou, S., "Hospital-acquired renal insufficiency," *Am. J. Kidney. Dis.* **39**(5), 930–936 (2002).
- [5] Seeliger, E., Sendeski, M., Rihal, C., and Persson, P., "Contrast-induced kidney injury: mechanisms, risk factors, and prevention," *Eur. Heart. J.* **33**(16), 2007–2015 (2012).
- [6] Bicknell, C., "Occupational radiation exposure and the vascular interventionalist," *Eur. J. Vasc.* **46**, 431 (2013).
- [7] Markelj, P., Tomažević, D., Likar, B., and Pernuš, F., "A review of 3D/2D registration methods for image-guided interventions," *Med. Image. Anal.* **16**(3), 642–661 (2012).
- [8] Carrell, T., Modarai, B., Brown, J., and Penney, G., "Feasibility and limitations of an automated 2D-3D rigid image registration system for complex endovascular aortic procedures," *J. Endovasc. Ther.* **17**(4), 527–533 (2010).
- [9] Penney, G., Weese, J., Little, J., Desmedt, P., Hill, D., et al., "A comparison of similarity measures for use in 2D/3D medical imageregistration," *IEEE Trans. Med. Imag.* **17**(4), 586–595 (1998).
- [10] Penney, G., Varnavas, A., Dastur, N., and Carrell, T., "An image-guided surgery system to aid endovascular treatment of complex aortic aneurysms: description and initial clinical experience," in [IPCAI], **6689**, 13–24 (2011).
- [11] Yushkevich, P. A., Piven, J., Hazlett, H. C., Smith, R. G., Ho, S., Gee, J. C., and Gerig, G., "User-guided 3D active contour segmentation of anatomical structures: significantly improved efficiency and reliability," *Neuroimage* **31**(3), 1116–1128 (2006).
- [12] Rohr, K., Fornefett, M., and Stiehl, H. S., "Approximating thin-plate splines for elastic registration: Integration of landmark errors and orientation attributes," in [Inf. Process. Med. Imaging], **1613**, 252–265, Springer (1999).
- [13] Guyot, A., Varnavas, A., Carrell, T., and Penney, G., "Non-rigid 2D-3D registration using anisotropic error ellipsoids to account for projection uncertainties during aortic surgery," in [MICCAI], **8151**, 179–186, Springer (2013).